IEEE Access
Multidisciplinary | Rapid Review | Open Access Journal

Received December 10, 2018, accepted December 18, 2018, date of publication December 26, 2018,
date of current version January 16, 2019.

Digital Object Identifier 10.1109/ACCESS.2018.2889498

Noncoherent Detection With Polar Codes

CHAOFAN CHEN[1], LI LI[2], LI WANG[3], (Member, IEEE), SHUAI WANG[1], (Member, IEEE), XIANGMING LI[1], (Member, IEEE), AND GEORGE K. KARAGIANNIDIS[4], (Fellow, IEEE)

[1]School of Information and Electronics, Beijing Institute of Technology, Beijing 100081, China
[2]Provincial Key Laboratory of Information Coding and Transmission, Southwest Jiaotong University, Chengdu 610031, China
[3]Research and Development Center, Huawei Technologies, 16494 Stockholm, Sweden
[4]Department of Electrical and Computer Engineering, Aristotle University of Thessaloniki, 54124 Thessaloniki, Greece

Corresponding author: Li Li (ll5e08@home.swjtu.edu.cn)

This work was supported in part by the Joint Foundation of the NSFC and the General Purpose Technology Research Program under Grant U1636125, and in part by the NSFC under Grant 61501383, Grant U1734209, and Grant 61771051.

ABSTRACT Polar codes (PCs) have attracted significant attention in the last decade, especially after their adoption in the forthcoming 5G wireless networks. However, previous studies focused on coherent polar codes, which always rely on the strong assumption of available perfect channel state information. Instead, in this paper, we investigate the use of PCs in noncoherent systems. First, a binary differential phase shift keying (BDPSK) demodulator is concatenated with a polar decoder to form the noncoherent detector, where successive cancellation (SC) is applied. The simulation results demonstrate that the SC-based PCs for noncoherent detection have approximately a discrepancy of only 3 dB compared with the coherent counterpart in noncoherent channels. Furthermore, in order to further decrease this discrepancy, we replace the BDPSK demodulator with a soft-input soft-output (SISO) multiple symbol differential sphere decoding demodulator. Similarly, the SC-based PC decoder is replaced by the SISO belief propagation-based PC decoder, and by using this novel architecture, an iterative noncoherent detector is constructed. Benefiting from further invoking extrinsic information transfer chart tool and the dynamic window-size detection scheme, the performance of the proposed iterative noncoherent detector becomes competitive with its coherent one in practical applications, since the performance degradation is reduced to 1 dB.

INDEX TERMS Polar codes, noncoherent detection, SISO-MSDSD, iterative detection, EXIT chart.

I. INTRODUCTION

Polar codes (PCs), proposed by Arıkan [1], have attracted tremendous attention, due to the provable capacity-achieving capability as well as to low encoding and decoding complexity. Performance of polar codes employing various decoding algorithms, e.g. successive cancellation (SC), successive cancellation list (SCL) and stack decoding, were systematically investigated in the literature [1]–[4]. However, most of these works rely on coherent detection and hence, they assume available perfect channel state information (CSI). But, in many cases it may be an extreme challenge to obtain sufficiently accurate CSI, as for example in massive Multi-Input Multi-Output (mMIMO) systems over fast fading channels, where coherent detection becomes even inferior to noncoherent one [5]. Therefore, extending the application of polar codes to noncoherent systems is a great challenge for research.

The performance of coded noncoherent systems, for example, concatenating binary differential phase shift keying (BDPSK) with turbo [6] or with low-density parity-check (LDPC) codes [7] have been reported in [8]–[10]. Specifically, in [8] it was demonstrated that by using turbo codes the bit error rate (BER) discrepancy between noncoherent and coherent detection is around 3.5 dB over additive white Gaussian noise (AWGN) channels. In [9], this discrepancy becomes 2∼3 dB, after replacing turbo with LDPC codes. Finally, in [10], a further improvement of LDPC aided noncoherent detection is achieved by incorporating the proposed ''3-symbol-observations-interval-ID'' scheme. Following the same concept, the raised questions are: how much is this discrepancy if we consider polar codes? Is there any advanced system design, that could efficiently mitigate the performance loss of the polar coded noncoherent detection with respect to the coherent one? To the best of our knowledge, these important issues are still open problems.

The contributions of this paper can be summarized as follow:

1) For first time in the literature, we present the concept of polar coded noncoherent detection and demonstrate its practical performance. In the noncoherent detection architecture, we employ the SC based polar decoder, which presents

a discrepancy of only 3 dB, compared to the coherent one. Simulation results confirm this performance.

2) In order to improve the performance of the basic polar coded noncoherent detection, we propose a soft-in soft-output multiple symbol differential sphere decoding (SISO-MSDSD) algorithm [11] to replace the conventional BDPSK demodulation, and a BP-based polar decoder as the outer code in the iterative detection architecture. An improved performance is also confirmed through simulations.

3) A dynamic window-size scheme is invoked into SISO-MSDSD part to achieve a better balance between complexity and performance gain. During this process, the configurations of window-size are refined, based on the EXIT chart analysis.

The rest of this paper is organized as follows: In Section II, some fundamental techniques are introduced, including polar codes and the SISO-MSDSD algorithm. The proposed polar coded noncoherent detection architecture is presented in Section III, while the dynamic window-size scheme and the associated EXIT chart analysis are presented in Section IV. Numerical results and simulations are demonstrated in Section V, and the computational complexity of the proposed noncoherent detection schemes is evaluated in Section VI. Finally, we conclude this paper in Section VII.

II. PRELIMINARIES

A. NOTATIONS

Throughout this paper we use lower case bold letters to denote a row vector and a lower case letter with a subscript to represent the element of a vector. If x_i^j denote a row vector of $(x_i, x_{i+1}, \ldots, x_j)$, then $\mathbf{x}^*$ is the conjugate of $\mathbf{x}$. We use an upper case letter $\mathbf{X}$ to denote a matrix and a low case letter with a pair of subscript x_{ij} to represent an element of $\mathbf{X}$ at i^{th} row and j^{th} column. Additionally, the notation $\otimes$ is the Kronecker product and $\|\cdot\|$ denotes the cardinality of a set.

B. POLAR CODES AND ITS BASIC DECODING ALGORITHMS

Polar codes are feasible for binary-input discrete memoryless channels (B-DMC) $W : \mathcal{X} \to \mathcal{Y}$ with transition probabilities $W(y|x), x \in \mathcal{X}, y \in \mathcal{Y}$, where $\mathcal{X}$ is the input alphabet and $\mathcal{Y}$ the output alphabet. Through channel polarization, N binary-input coordinate channels $W_N^{(i)} : \mathcal{X} \to \mathcal{Y}^N \times \mathcal{X}^{i-1}$, $1 \le i \le N$, can be composed from N independent copies of B-DMC channel W, with transition probability given by

$$W_N^{(i)}(y_1^N, u_1^{i-1}|u_i) \triangleq \sum_{u_{i+1}^N \in \mathcal{X}^{N-i}} \frac{1}{2^{N-1}} W_N(y_1^N|u_1^N), \quad (1)$$

where $W_N(y_1^N|u_1^N)$ refers to the combined channel between original bit sequence u_1^N and received signal y_1^N [1], and u_i, (y_1^N, u_1^{i-1}) are the input and output of the coordinate channel $W_N^{(i)}$, respectively.

The key principle of polar coding is always to select ''rich'' coordinate channels to transmit information bits. The rest ''poor'' coordinate channels carry only fixed bits, whose value is already known by the receiver. Since polar codes belong to linear block codes (LBC), it can be simply specified by its generator $N \times N$ matrix, $\mathbf{G_N} = \mathbf{B_N}\mathbf{F}^{\otimes \mathbf{n}}$. In more detail, for any $n \in \mathbb{N}$, let $N = 2^n$ denote the code length and $K < N$ the information bits length. Then, $\mathbf{B_N}$ is a bit-reversal permutation matrix that turns the n bits binary representation of an integer i, from $b_{n-1}, b_{n-2}, \ldots, b_0$ into $b_0, b_1, \ldots, b_{n-1}$. The $\mathbf{F}^{\otimes \mathbf{n}} = \mathbf{F} \otimes \mathbf{F}^{\otimes \mathbf{n-1}}$ is the n^{th} order Kronecker power, where $\mathbf{F}$ is the kernel matrix of $\left(\begin{smallmatrix} 1 & 0 \\ 1 & 1 \end{smallmatrix}\right)$. Thus, the polar encoding process can be described as

$$x_1^N = u_1^N \mathbf{G_N} = u_1^N \mathbf{B_N} \mathbf{F}^{\otimes \mathbf{n}}, \quad (2)$$

where x_1^N and u_1^N are the encoded and the original bit sequences, respectively. The original bit sequence u_1^N consists of two parts: the *information bits*, namely $u_{\mathcal{A}}$, and the *frozen bits*, which have constant value of zero, namely $u_{\mathcal{A}^C}$. In more detail, $\mathcal{A} \subset \{1, 2, \ldots, N\}$, $\|\mathcal{A}\| = K$ denotes the index set of information bits, and similarly, $\mathcal{A}^C$, $\|\mathcal{A}^C\| = N - K$ denotes the index set of frozen bits. Note that holds $\mathcal{A} \cup \mathcal{A}^C = \{1, 2, \ldots, N\}$.

SC and BP decoding algorithms are the two basic decoding methods for polar codes. SC decoding refers to a serial bit-by-bit hard decision algorithm and its latency is relative high. In contrast, BP decoding can be performed in parallel and hence satisfies high computational requirements, while, it is capable of providing soft output. Specifically, the factor graph used in BP decoding can be created from either the generator matrix or the parity-check matrix of the polar codes. Correspondingly, BP decoding can be categorized into generator matrix based, called as G-based BP, and parity-check matrix-based, called as H-based BP. All the aforementioned algorithms can be applied to noncoherent detection. We suggest the works [12]– [15] for more details about the above polar code decoding algorithms.

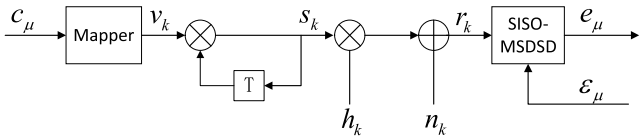

FIGURE 1. Noncoherent system with SISO-MSDSD detection.

C. SISO-MSDSD ALGORITHM

Next, we introduce the SISO-MSDSD algorithm proposed in [11]. First, we define the following column vectors

$$\begin{aligned} \mathbf{v} &= (v_{k-(D-2)}, v_{k-(D-3)}, \ldots, v_k)^T \\ \mathbf{s} &= (s_{k-(D-1)}, s_{k-(D-2)}, \ldots, s_k)^T \\ \mathbf{h} &= (h_{k-(D-1)}, h_{k-(D-2)}, \ldots, h_k)^T \\ \mathbf{n} &= (n_{k-(D-1)}, n_{k-(D-2)}, \ldots, n_k)^T \\ \mathbf{r} &= (r_{k-(D-1)}, r_{k-(D-2)}, \ldots, r_k)^T, \end{aligned} \quad (3)$$

which include $D - 1$ information symbols, D differentially modulated symbols, D channel coefficients, D AWGN samples and D received symbols, respectively. The value of D is determined by the number of jointly detected symbols in the SISO-MSDSD algorithm, which is also termed as detection ''window-size''. As shown in Fig. 1 the codeword bits c_μ is

mapped to M-ary PSK symbols v_k. Hence, it holds that

$$v_k \in \{e^{j2\pi m/M} | m = 0, 1, \ldots, M-1\}. \tag{4}$$

Then, the symbols are differentially modulated as

$$s_k = v_k s_{k-1}, s_0 = 1. \tag{5}$$

Compared with coherent detection, the conventional noncoherent detection scheme only incurs a 3 dB performance loss in AWGN channels. However, this performance loss will become significantly higher in fading channels. In order to recover this severe performance loss a SISO-MSDSD algorithm is proposed. Next, we mainly focus on Rayleigh fading channels. According to Clarke model [16], the autocorrelation function of h_k can be formulated as

$$\varphi_\kappa = E\{h_{k+\kappa} h_\kappa^*\} = J_0(2\pi B_f T_\kappa), \tag{6}$$

where $J_0(\cdot)$ denotes the zero-order first-kind Bessel function and $B_f T_\kappa$ (B_f is the maximum Doppler frequency shift) is the maximum normalized fading bandwidth. The received signal can be written as

$$r_k = h_k s_k + n_k, \tag{7}$$

where $n_k \sim \mathcal{CN}(0, \sigma_n^2)$ and its two-side power spectral density is N_0 (watts/Hz).

SISO-MSDSD algorithm is a modified version of MAP-MSDSD algorithm. The decision rule of MAP-MSDSD algorithm is based on searching the candidate vectors $\mathbf{v}$ and finding that which minimizes the metric

$$\hat{\mathbf{v}}_{MAP} = \arg\min_{\mathbf{v}} \{-\log(\Pr\{\mathbf{v}|\mathbf{r}\})\}. \tag{8}$$

Applying the Bayes' rule,

$$\begin{aligned} -\log(\Pr\{\mathbf{v}|\mathbf{r}\}) &\propto -\log(\Pr\{\mathbf{r}|\mathbf{v}\}) - \log(\Pr\{\mathbf{v}\}) \\ &\propto \|\mathbf{U}\mathbf{a}\|^2 - \log(\Pr\{\mathbf{v}\}), \end{aligned} \tag{9}$$

where $\mathbf{U}$ is a $D \times D$ upper triangular matrix, which can be derived from channel autocorrelation matrix[1] and received symbol sequence. Then, $\mathbf{a} \triangleq [a_1, a_2, \ldots, a_D]^T$ is the accumulative product of information symbols that obeys to

$$a_i = \begin{cases} \prod_{l=i}^{D-1} v_l^*, & 1 \le i \le D-1 \\ 1, & i = D. \end{cases} \tag{10}$$

Apparently, we can always achieve $\|\mathbf{U}\mathbf{a}\| \le R_m^2$, where R_m is normally regarded as the initial sphere radius of MAP-MSDSD. Finally, $\log(\Pr\{\mathbf{v}\})$ is an *a priori* information, which may be provided by outer code in the same iterative detection architecture.

Assuming that the elements of $\mathbf{v}$ are independent to each other, we can rewrite (9) as

$$\begin{aligned} &\|\mathbf{U}\mathbf{a}\|^2 - \log(\Pr\{\mathbf{v}\}) \\ &= \sum_{i=1}^{D-1} \left(\left| \sum_{\kappa=i}^{D} u_{i\kappa} a_\kappa \right|^2 - \log(\Pr\{v_i\}) \right) \\ &\le R_m^2 - |u_{DD}|^2 \triangleq R^2, \end{aligned} \tag{11}$$

where $u_{i\kappa}$ is the element of $\mathbf{U}$ in i^{th} row and κ^{th} column. From (11), MAP-MSDSD algorithm is equivalent to find a candidate vector $\mathbf{v}_{MAP}$ which results in the minimum sphere radius of R^2. In order to adapt (11) to formal sphere detection programming, it could be further represented as a recursive accumulation process as

$$\begin{aligned} d_i^2 &\triangleq \Delta_i^2 + d_{i+1}^2 \\ &= \underbrace{\left| u_{ii} a_{i+1} v_i^* + \sum_{\kappa=i+1}^{D} u_{i\kappa} a_\kappa \right|^2 - \log(\Pr\{v_i\})}_{\Delta_i^2} \\ &\quad + \underbrace{\sum_{\tau=i+1}^{D-1} \left(\left| \sum_{\kappa=\tau}^{D} u_{\tau\kappa} a_\kappa \right|^2 - \log(\Pr\{v_\tau\}) \right)}_{d_{i+1}^2} \le R^2, \end{aligned} \tag{12}$$

where $d_D^2 = 0$. The equivalence between (11) and (12) is revealed by the fact that $d_1^2 = \|\mathbf{U}\mathbf{a}\|^2 - \log(\Pr\{\mathbf{v}\})$.

Based on (12), MAP-MSDSD can be executed as follows: firstly, index i takes value of $D-1$ and the first potential information symbol $\hat{v}_{D-1}$, which satisfies $\Delta_{D-1}^2 = d_{D-1}^2 \le R^2$, can be found. Then, i decreases by one step and the second signal point $\hat{v}_{D-2}$, which satisfies $d_{D-2}^2 = \Delta_{D-2}^2 + d_{D-1}^2 \le R^2$ is found. we can generate a temporary hypothesis of the original information vector, which is represented by $\hat{\mathbf{v}} = (\hat{v}_1, \hat{v}_2, \ldots, \hat{v}_{D-1})^T$. Meanwhile, the sphere radius can be updated by $R^2 = d_1^2$. Next, the above entire process is executed again by adjusting the initial value of i to $D-2$. If a valid vector can be found in this second round, i.e. i decreases from $D-2$ to 1 and $d_i^2 \le R^2$ is always satisfied, then the sphere radius R^2 could be further reduced. Repeat above process until R^2 reaches its minimum value. The resultant last valid vector $\hat{\mathbf{v}}$ is the final decision made by MAP-MSDSD algorithm. This sphere detection process is also summarized by a pseudo code in [11].

SISO-MSDSD algorithm is obtained by simply substituting the decision metric of MAP-MSDSD algorithm shown in (12) to the log likelihood ratio calculation of an information bit. Consequently, in SISO-MSDSD algorithm, the *a posteriori* logarithm likelihood ratio (LLR) of an information bit c_μ can be expressed as

$$\begin{aligned} l_{c_\mu} &= \log\left(\frac{\Pr\{c_\mu = b|\mathbf{r}\}}{\Pr\{c_\mu = \bar{b}|\mathbf{r}\}} \right) \\ &\approx \log\left(\frac{\max_{\mathbf{v}:c_u=b}\{\exp(-\|\mathbf{U}\mathbf{a}\|^2 + \log(\Pr\{\mathbf{v}\}))\}}{\max_{\mathbf{v}:c_u=\bar{b}}\{\exp(-\|\mathbf{U}\mathbf{a}\|^2 + \log(\Pr\{\mathbf{v}\}))\}} \right) \\ &= -\|\mathbf{U}\hat{\mathbf{a}}_{MAP}^b\|^2 + \log(\Pr\{\hat{\mathbf{v}}_{MAP}^b\}) \\ &\quad + \|\mathbf{U}\hat{\mathbf{a}}_{MAP}^{\bar{b}}\|^2 - \log(\Pr\{\hat{\mathbf{v}}_{MAP}^{\bar{b}}\}), \end{aligned} \tag{13}$$

where b and $\bar{b}$ are binary 0 and 1, respectively, $\mathbf{v}: c_\mu = b$ indicates the set of all the information vectors, whose μ^{th} element is 0. Correspondingly, $\hat{\mathbf{v}}_{MAP}^b$ is the optimum information

[1]The channel autocorrelation matrix can be obtained from (6). The detailed derivation and evaluation of $\mathbf{U}$ can be found in [21].

vector selected from the set $\mathbf{v}: c_\mu = b$, which maximizes the numerator in (13).

Moreover, the *a priori* LLR of bit c_μ is defined as

$$\varepsilon_{c_\mu} = \log\left(\frac{\Pr\{c_\mu = b\}}{\Pr\{c_\mu = \bar{b}\}}\right). \tag{14}$$

Apparently, the *extrinsic* LLR of bit c_μ can be obtained as

$$e_{c_\mu} = l_{c_\mu} - \varepsilon_{c_\mu}. \tag{15}$$

Hence, SISO-MSDSD algorithm is capable of operating the *a priori* LLR input by another component in iterative detection architecture and then feeding back the *extrinsic* LLR.

III. SYSTEM MODEL

In order to appropriately extend the application of polar codes to noncoherent scenarios, we conceive two distinct detection architectures. The first employs a serial detection architecture, where the conventional differential demodulator is concatenated with the SC decoding algorithm, which is based on a polar decoder. This detection architecture is also termed as the "basic noncoherent detection". In order to further improve its BER performance, we transform the architecture of this basic noncoherent detection to an iterative manner, which constitutes the "iterative noncoherent detection".

A. BASIC NONCOHERENT DETECTION ARCHITECTURE

In order to adapt polar coding to noncoherent scenarios, where the channel state information is not available, we differentially modulate the encoded bits, $\mathbf{c} = (c_1, c_2, \ldots, c_N)$, at the transmitter. At the receiver, the received signals $\mathbf{r} = (r_1, r_2, \ldots, r_{N+1})$ first are processed by a differential demodulator. Then, a polar decoder is concatenated with this preceding differential demodulator for further tackle with its output data stream, namely $\mathbf{y} = (y_1, y_2, \ldots, y_N)$. Finally, the polar decoder makes a decision and a hypothesis of the original information bits, namely $\hat{\mathbf{u}} = (\hat{u}_1, \hat{u}_2, \ldots, \hat{u}_K)$ is produced. This basic noncoherent detection architecture is depicted in Fig. 2.

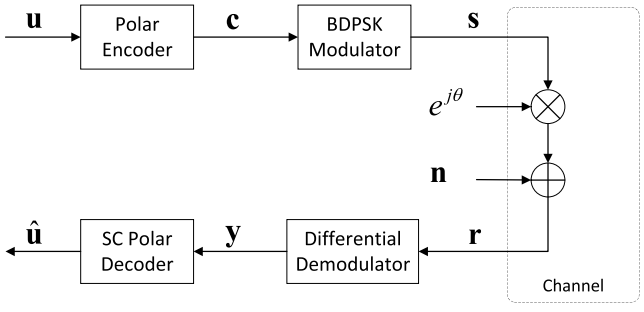

FIGURE 2. Basic noncoherent detection architecture.

Normally, the conventional demodulator will generate hard decisions. However, the decoding procedure of polar code relies on the initial likelihoods of its encoded bits $\mathbf{c} = (c_1, c_2, \ldots, c_N)$. Hence, in order to successfully support the basic noncoherent detection, the differential demodulator shown in Fig. 2 has to appropriately evaluate the likelihoods of each encoded bits and sends these soft-outputs to concatenated polar decoder. This critical challenge involved in basic noncoherent detection can be solved as follows. Firstly, the signals received from channel are directly input to differential demodulator. Then, the differential demodulator multiplies the conjugate of $(k-1)^{th}$ signal of r_{k-1} by the consecutive k^{th} signal of r_k, and calculates the real part of this product. The associated result is given by

$$y_k = \Re\{r_{k-1}^* r_k^*\}, \tag{16}$$

where r_{k-1}^* represents the conjugate of r_{k-1}, $\Re\{\cdot\}$ denotes the real part of a complex number, and y_k in (16) constitutes the initial soft-output of the differential demodulator. However, as stated above, the likelihood of each encoded bit c_k is provided to polar decoder. Hence we should correctly convert this initial soft-output of differential demodulator to the likelihood of c_k. Since the channel is assumed to be a noncoherent one, *i.e.* an AWGN channel, on which a random phase distortion is further imposed, according to [8], the probability density function (pdf) of y_k while c_k is given approximately obeys to a Gaussian distribution. Hence, $P(y_k|c_k = i) \sim N(\mu_i, \sigma_0^2)$, where $i \in \{0, 1\}$, $\mu_i = 1 - 2i$, and $\sigma_0^2 = N_0 + (N_0/2)^2$. Therefore, the initial LLR of an encoded bit c_k can be evaluated as

$$L(c_k) = \ln\frac{P(y_k|c_k=0)}{P(y_k|c_k=1)} = \ln\frac{\frac{1}{\sqrt{2\pi\sigma_0^2}}e^{-\frac{(y_k-u_0)^2}{2\sigma_0^2}}}{\frac{1}{\sqrt{2\pi\sigma_0^2}}e^{-\frac{(y_k-u_1)^2}{2\sigma_0^2}}} = 2 * y_k/\sigma_0^2. \tag{17}$$

The LLR values of $L(c_k)$ obtained from (17) are acting as the soft-input required by the polar code. Hence the early mentioned challenge can be resolved.

Furthermore, it has been reported in [17] and [18] that in non-iterative detection architecture, the SC decoding algorithm outperforms BP decoding algorithm. Hence, in the basic noncoherent detection architecture of Fig. 2, we opt for SC decoding algorithm for the polar decoder.

In order to evaluate the efficiency of the basic noncoherent iterative detection, the associated BER performance is demonstrated in Fig. 3. In more detail, according to the same construction method proposed in [1], three kinds of polar codes are constructed. They are only different in codeword length and termed as $\mathcal{C}_1(256, 128)$, $\mathcal{C}_2(512, 256)$ and $\mathcal{C}_3(1024, 512)$, respectively. Then, a transceiver consisting of polar encoder, BPSK modulation, BPSK demodulation, as well as SC decoding algorithm based polar decoder is regarded as our coherent counterpart. In this coherent system, perfect CSI is assumed.

It can be observed from Fig. 3 that the basic noncoherent detection requires only an Eb/N0 less than 7 dB to achieve a very low BER level of 10^{-4}. But in contrast to its coherent counterpart, there is always about 3 dB performance loss,

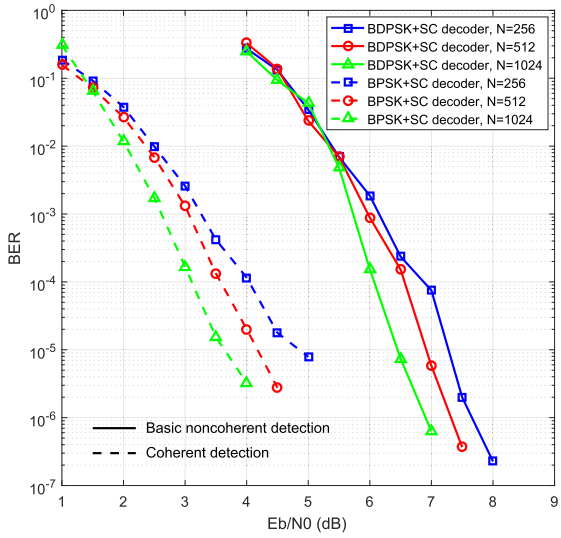

FIGURE 3. BER performance comparison between the basic noncoherent detection and its coherent counterpart. Different polar codes of $\mathcal{C}_1$, $\mathcal{C}_2$ and $\mathcal{C}_3$ are considered in this comparison.

regardless of the length of polar code employed. In order to combat with this performance discrepancy, we further improve the noncoherent detection in Section III-B.

B. ITERATIVE NONCOHERENT DETECTION ARCHITECTURE

In order to improve the performance of the basic noncoherent detection architecture shown in Fig. 2, we further invoke the powerful iterative detection strategy. Normally, an iterative detector consists of two components, namely *inner decoder* and *outer decoder* [19]. Both of them shall be capable of accepting soft-inputs and generating soft-output, and then they exchange their information. Apparently, the differential demodulator shown in Fig. 2 has only a single input stream, which is the signals received from the channel. Hence, it cannot additionally allow the SC polar decoder to input feedback information. Meanwhile, the SC polar decoder neither has the ability of feeding back information to preceding demodulator. According to the above analysis, the basic noncoherent detection architecture shown in Fig. 2 cannot realize the information exchange between two detection components. Hence it does not support iterative detection manner.

Accordingly, we replace the differential demodulator shown in Fig. 2 by its more powerful counterpart SISO-MSDSD algorithm based demodulator. Because, as explained by the sentences under eq.(15) in Section II-C, SISO-MSDSD algorithm is capable of generating *extrinsic information* based on input *a priori* information. Hence it can support iterative detection and we could utilize it as the inner decoder. Furthermore, we also replace the SC polar decoder by the BP decoding algorithm based polar decoder. Because, only the BP polar decoder is capable of feeding back information to the preceding detection component. The BP polar decoder will act as the outer decoder in the iterative detection architecture. Finally, at the transmitter, an interleaver is deployed between the polar encoder and the differential modulator.

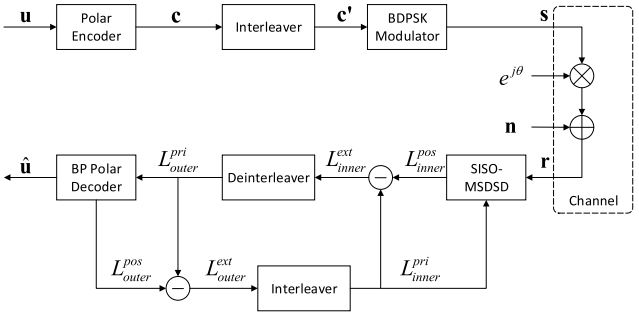

FIGURE 4. Iterative noncoherent detection architecture.

This interleaver is invoked for omitting the time-correlation of the channel. Symmetrically, at the receiver, a deinterleaver and an interleaver are deployed between the SISO-MSDSD and the BP polar decoder. After above-mentioned developments, we construct the basic architecture of our iterative noncoherent detection, which is depicted in Fig. 4.

As it is observed from Fig. 4, in one iteration procedure, SISO-MSDSD first generates its soft-output according to eq. (13). Apparently, this procedure will rely on the signal sequence $\mathbf{r}$ received from the channel and on the *a priori* LLRs L_{inner}^{pri} obtained from the BP polar decoder in the last iteration. Accurately, this soft-output is the *a posteriori* LLRs L_{inner}^{pos} of the encoded and then interleaved codeword $\mathbf{c}'$. By subtracting L_{inner}^{pri} from L_{inner}^{pos}, we obtain the *extrinsic* LLRs L_{inner}^{ext}. Then, after deinterleave operation, L_{inner}^{ext} is converted to the *a priori* LLRs of the BP polar decoder. Based on this *a priori* information, BP polar decoder is capable of updating its *a posteriori* LLRs L_{outer}^{pos}. Similarly, after subtracting the *a priori* LLRs L_{outer}^{pri} from L_{outer}^{pos}, we obtain the updated *extrinsic* LLRs L_{outer}^{ext}. The interleaved version of L_{outer}^{ext} will act as the *a priori* information for SISO-MSDSD in the next iteration. The above-mentioned data-stream operation procedure will be repeated until the estimated bit-sequence is a legitimate polar encoded codeword or the maximum iteration number is exhausted.

The iterative noncoherent detection architecture shown in Fig. 4 can be further improved by appropriately selecting the BP polar decoding algorithm. This issue will be discussed in Section IV. Then, as mentioned early in this sub-section, iterative noncoherent detection is capable of outperforming the basic noncoherent detection. This fact will be verified through our abundant numerical simulations in Section V.

IV. EXIT CHART ANALYSIS

As reported in [5], [11], [20], and [21], the performance of SISO-MSDSD is dominated by the detection window-size. A significant performance gain can be obtained by increasing its window-size, but at the cost of computational complexity. Hence a dynamic window-size scheme is employed into the iterative noncoherent detection system for achieving a good tradeoff between performance and complexity. On the other hand, EXIT chart [22] is a low-complexity high-accuracy

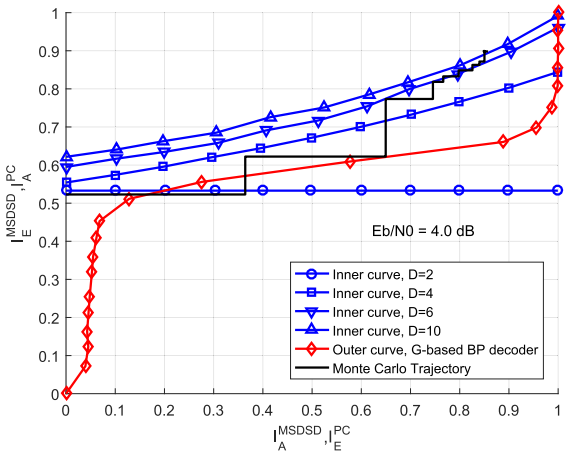

FIGURE 5. EXIT chart analysis of the iterative noncoherent detection scheme using G-based BP polar decoder at Eb/N0 of 4 dB.

analysis tool to reveal the characteristics of an iterative detection. Hence we employ it to guide our dynamic window-size design.

Without loss of generality, we use a window-size candidate pool of {2, 4, 6, 10} and a (256, 128) polar code to illustrate the EXIT chart assisted dynamic window-size design procedure. For example, an EXIT chart of the iterative noncoherent detection over noncoherent AWGN channel [11] with SNR per bit of $Eb/N0 = 4.0$ dB is illustrated in Fig. 5. In this figure the blue curves represent the *extrinsic information* increasing trace of the SISO-MSDSD component while increasing its input *a priori information*, which are also called the inner curves. The red curve depicts the *extrinsic information* increasing trace of the polar code component, which is also called the outer curve.

The principle of EXIT chart [23] points out that the more the intersection between inner curve and outer curve get close to (1, 1) point of EXIT chart, the better the BER performance will be. According to this principle and observe at Fig. 5 again that when window-size is 2, the blue curve labeled by circles and the red curve will intersect at (0.2, 0.52) point, which is still far away from (1, 1) point and implies a poor BER performance. When the window-size increases from 4 to 6 and further to 10, the open tunnel between inner and outer curves occurs. Meanwhile, their intersection point get more and more close to perfect (1, 1) point, which implies an improved BER performance.

The above-mentioned EXIT chart performances inspire us to adopt a short window-size during early iterations. Then, along with the increase of iterations, the inner curve trend to intersect the outer curve. However, if we appropriately increase the window-size in the forthcoming iterations, this intersection can be avoided. As a benefit, we achieve the same BER performance as that uses a fixed large window-size in every iteration, but significantly reduce the computational complexity. This strategy constructs our EXIT chart assisted dynamic window-size design.

Consequently, according to the guidance of EXIT chart curves in Fig. 5, the dynamic window-sizes during 10 iterations are consecutively set to be [2, 4, 6, 6, 6, 6, 6, 6, 10, 10]. The detection trajectory represented by a black curve in Fig. 5 is generated by Monte Carlo simulations, which indicates the practical detection results. In Fig. 5, the detection trajectory indeed moves towards (1, 1) point but still cannot approach. It implies that the entire system will occur an error floor at the current power budget of $Eb/N0 = 4.0$. Hence, in Fig. 6∼7, we gradually increase the signal power and find that the $Eb/N0$ threshold should be 5 dB for enabling the trajectory to finally arrive at the perfect (1, 1) point in EXIT chart.

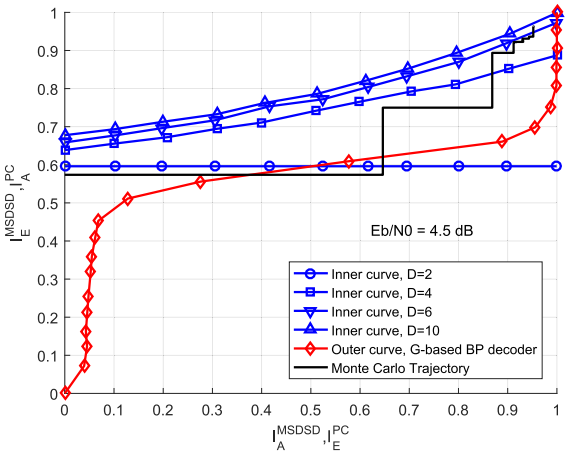

FIGURE 6. EXIT chart analysis of the iterative noncoherent detection scheme using G-based BP polar decoder at Eb/N0 of 4.5 dB.

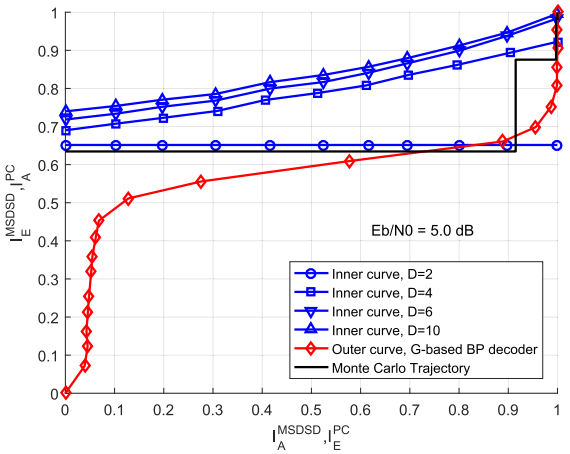

FIGURE 7. EXIT chart analysis of the iterative noncoherent detection scheme using G-based BP polar decoder at Eb/N0 of 5 dB.

The above-mentioned dynamic window-size design aims at improving the iterative noncoherent detection by adjusting the inner curve in EXIT chart. Alternatively, we could also improve the iterative noncoherent detection by adjusting the outer curve, i.e. we could replace the G-based BP decoder employed in Fig. 5∼7 by the H-based version. The resultant EXIT charts are as shown in Fig. 8∼10. It can be seen from these figures that the outer curve corresponding

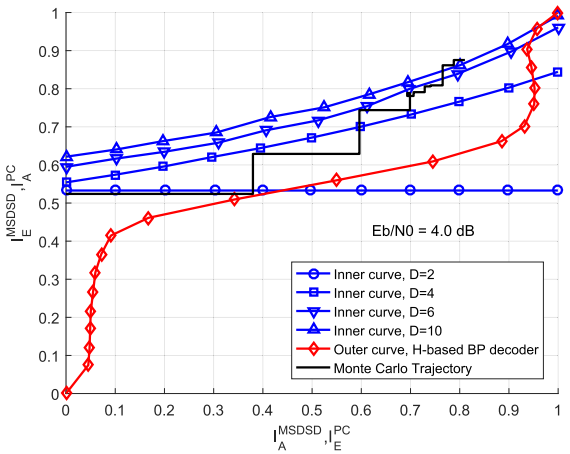

FIGURE 8. EXIT chart analysis of our iterative noncoherent detection using H-based BP polar decoder at Eb/N0 of 4 dB.

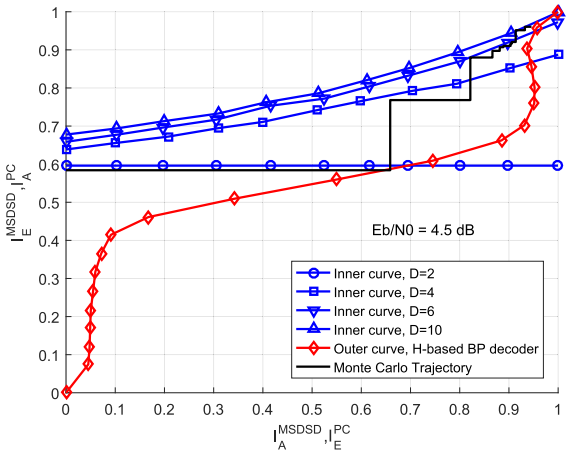

FIGURE 9. EXIT chart analysis of our iterative noncoherent detection using H-based BP polar decoder at Eb/N0 of 4.5 dB.

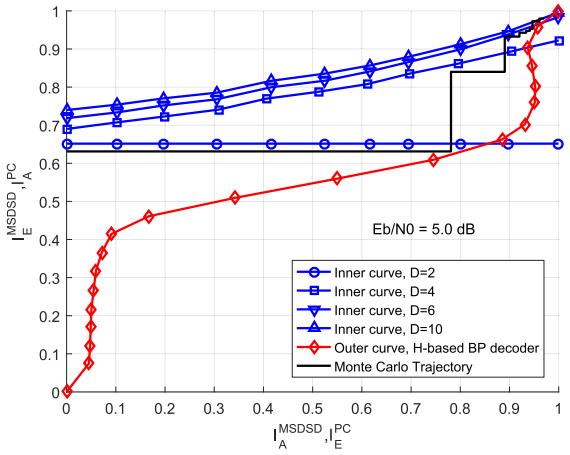

FIGURE 10. EXIT chart analysis of our iterative noncoherent detection using H-based BP polar decoder at Eb/N0 of 5 dB.

to H-based BP decoder achieves a higher slope than its counterpart in Fig. 5∼7, especially for the top-right part. This phenomenon implies that the intersection between inner and outer curves in Fig. 8∼10 will get more close to (1, 1) point. We will verify this conclusion in the next section.

V. NUMERICAL RESULTS AND SIMULATIONS

The Monte Carlo based simulation results of basic noncoherent detection presented in Section III-A, and that of iterative noncoherent detection in Section III-B, as well as that of coherent detection counterpart are demonstrated and compared in this section. The parameters used in our simulations are summarized in Table 1.

TABLE 1. Simulation parameters.

Parameter		Description
Channel		Noncoherent AWGN with Phase distortion [11]
Modulations		BPSK, BDPSK
G-based BP stop criterion		G-matrix early stopping criterion [24]
H-based BP stop criterion		All check equations are satisfied or maximum iteration is exhausted
Polar Code configurations		$\mathcal{C}_1$, $\mathcal{C}_2$ and $\mathcal{C}_3$
Max. iteration used within G-based BP	in iterative noncoherent detection	20
Max. iteration used within H-based BP	in coherent detection	200
	in iterative noncoherent detection	20
Max. iteration used between SISO-MSDSD and BP polar decoder		20
SISO-MSDSD window-sizes		2, 4, 6, 10
Simulation Samples		Guarantee detected Error Number > 500

Firstly, the polar decoder in our iterative noncoherent detection architecture can either rely on the G-based BP algorithm or on the H-based BP algorithm. The comparison between their EXIT charts has been portrayed in Section IV, which reasonably anticipates that employing H-based BP algorithm will achieve a better performance, especially for moderate and large SISO-MSDSD window-size. Correspondingly, the comparison between their practical BER performance is illustrated in Fig. 11. Observe at Fig. 11 that employing H-based BP polar decoder in iterative noncoherent detection architecture constantly outperforms employing G-based BP polar decoder while window-size is fixed to 4, 6. An around 0.5 dB performance gain is achieved at the target BER of 10^{-5}. These practical BER performances coincide with our previous EXIT chart analyses. Hence, in our ensuing simulations, the polar decoding algorithm employed in iterative noncoherent detection and in coherent detection will be fixed to H-based BP.

Then, it is demonstrated in Fig. 12 that with the aid of SC polar decoder, our basic noncoherent detection is capable of reducing the performance loss to 3 dB compared to the coherent detection counterpart. Furthermore, in order to enhance the performance of noncoherent detection, we further invoked the iterative detection architecture in Section III-B. Its efficiency is confirmed in Fig. 12 that the resultant iterative noncoherent detection further reduces the above-mentioned performance loss to 2 dB by

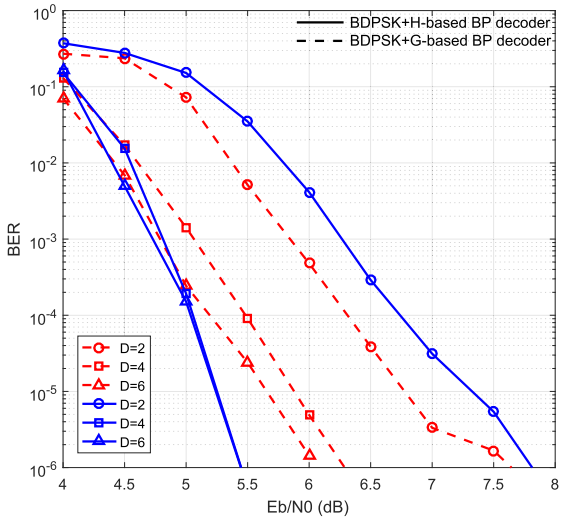

FIGURE 11. BER performance comparison between employing G-based BP and employing H-based BP in iterative noncoherent detection architecture. Polar code configuration of $\mathcal{C}_3$ is used.

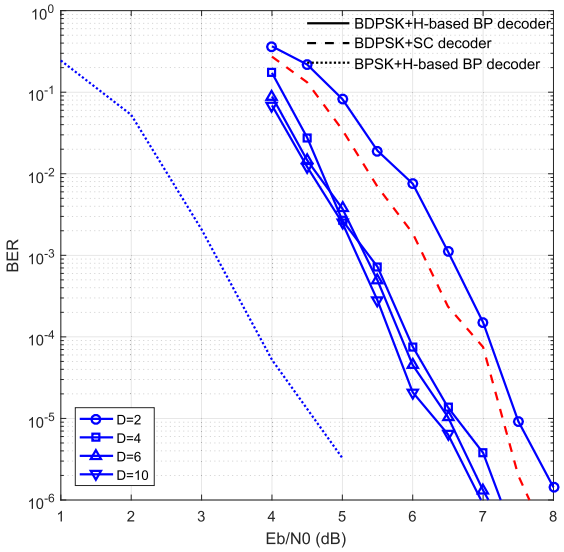

FIGURE 12. BER performance comparison. Polar code configuration of $\mathcal{C}_1$ is employed.

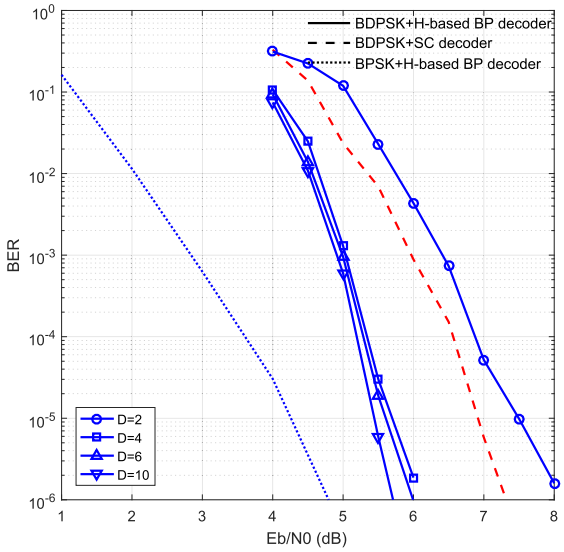

FIGURE 13. BER performance comparison. Polar code configuration of $\mathcal{C}_2$ is employed.

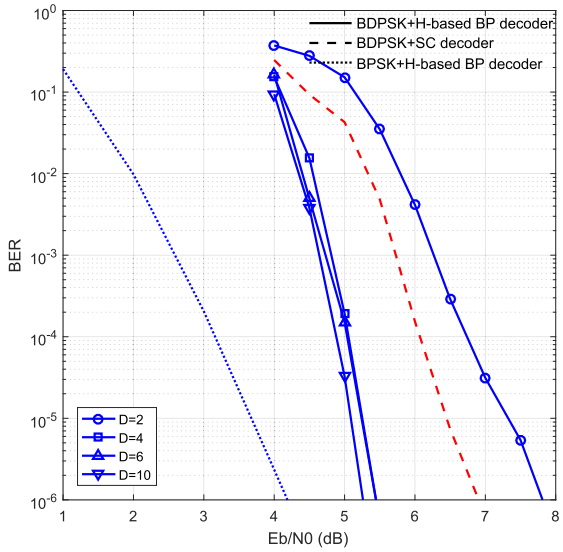

FIGURE 14. BER performance comparison. Polar code configuration of $\mathcal{C}_3$ is employed.

gradually enlarging the SISO-MSDSD detection window-size from 2 to 10.

Similar phenomenon is observed in Fig. 13 and Fig. 14 again, where the polar code configuration of $\mathcal{C}_1$ is replaced by $\mathcal{C}_2$ and $\mathcal{C}_3$, respectively. Particularly, in these cases, where longer polar codewords are used, we can reduce the performance loss of noncoherent detection with respect to its coherent counterpart as small as around 1 dB at the target BER of 10^{-6}.

On the other hand, while focusing on the performance of iterative noncoherent detection shown in Fig. 12∼14, it is clear that the performance gain achieved by increasing the window-size becomes more and more marginal. Meanwhile, the system computational complexity is sensitive to the window-size employed in SISO-MSDSD. Hence, a dynamic SISO-MSDSD window-size scheme is proposed for our iterative noncoherent detection architecture in previous Section IV. Herein, with the dynamic window-size sequence of [2,4,6,6,6,6,6,6,10,10], its BER performance is compared with that of the fixed window-size schemes in Fig. 15. Observe at Fig. 15 that the dynamic window-size scheme almost achieves the same performance as that of fixed window-size scheme having a large window-size of 10 upon SNR $>$ 5.5 dB. But, bear in mind that, dynamic window-size scheme imposes relatively less computational complexity owing to using small and moderate SISO-MSDSD window-sizes in early iterations.

Hence, according to the complexity performance, which will be discussed later in Section VI, we may propose to employ the dynamic window-size scheme based iterative

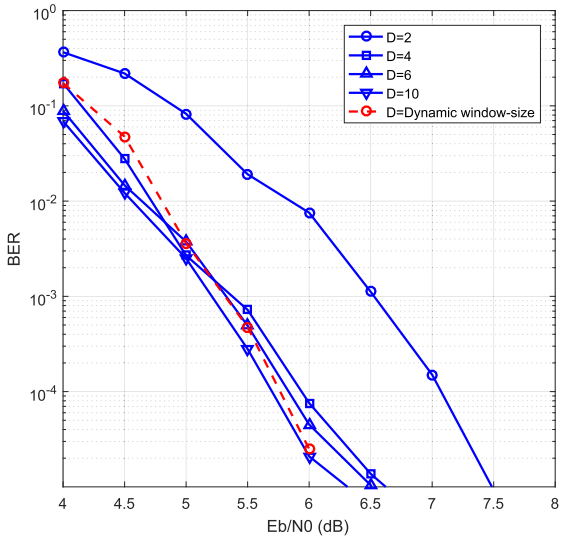

FIGURE 15. BER performance comparison between dynamic window-size detection and fixed window-size detection. Polar code configuration of $\mathcal{C}_1$ is employed.

noncoherent detection for achieving a good trade-off between BER performance and system computational complexity.

VI. COMPLEXITY ANALYSIS

Beside the BER performance, the required computational complexity is another critical metric for assessing a detection scheme. In this section, we analyze and evaluate the imposed complexity of the proposed detection schemes: the basic noncoherent and the iterative noncoherent detection. Furthermore, similar to [11], the average number of real-valued multiplicative operations (RMO) required to produce one soft-output value (or one hard decision) is used as the complexity metric.

Next, we consider our basic noncoherent detection. Apparently its complexity consists of two parts. One part is imposed by the conventional differential detection. As indicated in Section III-A, the differential detection could be considered as an $\Re\{\cdot\}$ operation, which requires two RMOs in average to make a decision. Hence, according to the definition of complexity metric, the complexity of this part is 2. The other part is imposed by the SC based polar decoding. According to [1], in order to evaluate the likelihood ratios of N input bits of a polar code, the number of required RMOs is $\mathcal{O}(N \log N)$. Therefore, the entire complexity of the basic noncoherent detection scheme can be approximated as

$$C_{basic} \simeq 2 + \mathcal{O}(\log N), \tag{18}$$

where N is the length of a polar codeword.

Then, we attempt to quantify the complexity of the iterative noncoherent detection, which also consists of two parts. The first part is imposed by the SISO-MSDSD detector. According to [11], its complexity is dominated by the calculation of eq. (12) in Section II-C. In order to evaluate Δ_i^2 in eq. (12) once, a number of $4(D-i)+6$ RMOs is required. In more detail, the calculation of $\sum_{\kappa=i+1}^{D} u_{i\kappa} a_\kappa$ requires $4(D-i)$ RMOs and that of $\left|u_{ii} a_{i+1} v_i^* + p\right|^2$ requires 6 RMOs. Then, during the SISO-MSDSD detection procedure, d_i^2 in eq. (12) has to be frequently updated. However, the number of repeated implementations of eq. (12) is not a constant, and is affected by the window-size D and the *a priori* information I_A^{MSDSD} input to SISO-MSDSD. Hence, instead of formulating the complexity measurement metric of the SISO-MSDSD part, we provide its practical simulation results in Fig. 16, where different configurations of the detection window-size D and *a priori* information amounts of $I_A^{MSDSD} = [0, 0.1, 0.2, 0.3, 0.4, 0.5, 0.6, 0.7, 0.8, 0.9, 0.99, 0.999, 1.0]$ are tested. It can be observed from Fig. 16 that the complexity of SISO-MSDSD is dramatically increased by extending the window-size, which is the major reason that we invoke the dynamic window-size scheme in Section IV, as well as in Fig. 15. Meanwhile, the complexity could be mitigated by having high *a priori* information, which is actually associated with a high $Eb/N0$ configuration.

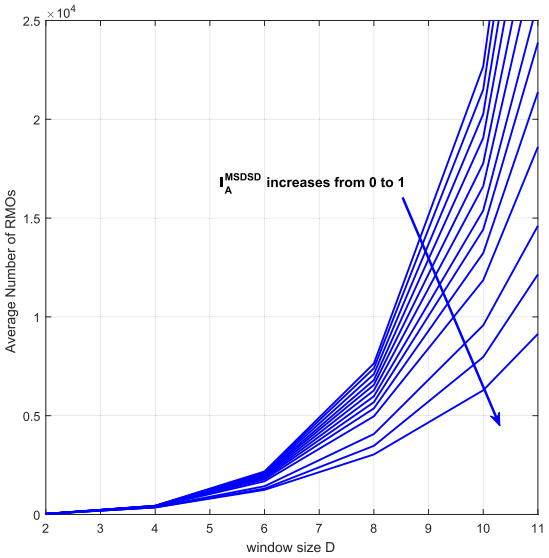

FIGURE 16. Complexity of the SISO-MSDSD scheme.

The second part is imposed by the H-based BP polar decoding. Since it belongs to BP algorithm, its complexity is related to the average number of inner iterations I_{inner} and outer iterations I_{outer} required for detecting one codeword. Its complexity is also related to the average degree of check nodes $\bar{d}_c$. According to [25], approximate $\mathcal{O}(I_{outer} I_{inner} N(N-K)(\bar{d}_c - 2))$ RMOs are required for the BP decoder to detect a single codeword, where N, K are the codeword length and number of information bits, respectively. In more detail, the average number of I_{inner} and I_{outer} required for decoding a polar codeword is affected by the practical $Eb/N0$ condition and SISO-MSDSD window-size. Hence, we illustrate some practical values of I_{inner} and I_{outer} in Table 2, where the polar code configuration of $\mathcal{C}_1$ is employed. From this table it is evident that along with an increase of the signal power,

TABLE 2. Practical test of I_{inner} and I_{outer} during H-based BP polar decoder.

$N-K$	D	$\bar{d}_c$	$I_{outer}I_{inner}$			
			Eb/N0= 4 dB	Eb/N0= 5 dB	Eb/N0= 6 dB	Eb/N0= 7 dB
128	2	3.5	365.14	154.49	28.36	8.57
128	4	3.5	175.93	22.57	10.07	7.35
128	6	3.5	115.35	20.39	9.46	7.05
128	10	3.5	101.5	17.49	9.06	6.87

the iterations required by BP decoding will be significantly reduced.

Therefore, the entire complexity of the proposed iterative noncoherent scheme can be approximated as

$$C_{iterative} = \mathcal{O}\left(I_{outer}I_{inner}(N-K)(\bar{d}_c-2)\right) + I_{outer}C_{MSDSD}. \quad (19)$$

According to above, the iterative noncoherent detection may result in a much higher complexity compared to the basic noncoherent detection, even dynamic window-size scheme is exploited in the last one. However, the BP polar decoding employed in iterative noncoherent detection can be implemented in a fully parallel mode. In contrast, the SC polar decoding employed in basic noncoherent detection has to be executed in a serial mode. Hence, the proposed iterative noncoherent detection is proper for applications with demands both high performance and low processing latency, while being tolerant of a high computational complexity.

VII. CONCLUSION

In this paper, we have extended the use of polar codes in cases where accurate channel estimation is unfeasible, by proposing noncoherent detection. We have first designed the basic noncoherent detection scheme, where polar decoding is using according to the SC algorithm. Then, in order to further improve the performance of noncoherent detection, we have applied iterative noncoherent detection, where the BP decoding algorithm is employed. Furthermore, EXIT chart tool has been invoked, which reveals that H-based BP decoding outperforms G-based BP decoding in our scenarios. The associated BER simulations confirm the efficiency of the proposed noncoherent detection schemes. Complexity issues have been investigated and a dynamic window-size detection scheme has been proposed to reduce the system complexity.

REFERENCES

[1] E. Arıkan, "Channel polarization: A method for constructing capacity-achieving codes for symmetric binary-input memoryless channels," *IEEE Trans. Inf. Theory*, vol. 55, no. 7, pp. 3051–3073, Jul. 2009.
[2] W. Xu, Z. Wu, Y.-L. Ueng, X. You, and C. Zhang, "Improved polar decoder based on deep learning," in *Proc. IEEE Int. Workshop Signal Process. Syst.*, Lorient, France, Oct. 2017, pp. 1–6.
[3] I. Tal and A. Vardy, "List decoding of polar codes," *IEEE Trans. Inf. Theory*, vol. 61, no. 5, pp. 2213–2226, May 2015.
[4] K. Niu and K. Chen, "Stack decoding of polar codes," *Electron. Lett.*, vol. 48, no. 12, pp. 695–697, Jun. 2012.
[5] D. Raphaeli, "Noncoherent coded modulation," *IEEE Trans. Commun.*, vol. 44, no. 2, pp. 172–183, Feb. 1996.
[6] C. Berrou, A. Glavieux, and P. Thitimajshima, "Near Shannon limit error-correcting coding and decoding: Turbo-codes. 1," in *Proc. IEEE Int. Conf. Commun.*, Geneva, Switzerland, May 1993, pp. 1064–1070.
[7] R. G. Gallager, "Low-density parity-check codes," *IRE Trans. Inf. Theory*, vol. 8, no. 1, pp. 21–28, Jan. 1962.
[8] E. K. Hall and S. G. Wilson, "Turbo codes for noncoherent channels," in *Proc. IEEE Globecom Commun. Theory Miniconf.*, Phoenix, AZ, USA, Nov. 1997, pp. 66–70.
[9] E. Mo and P. Y. Kam, "Log-likelihood metrics based on two-symbol-interval observations for LDPC codes with BDPSK transmission," in *Proc. IEEE 68th Veh. Technol. Conf.*, Calgary, BC, Canada, Sep. 2008, pp. 1–5.
[10] J. Zhang and P.-Y. Kam, "Iterative decoding of LDPC-coded BDPSK with new LLR metric over the noncoherent channel," in *Proc. IEEE Int. Conf. Commun.*, Kyoto, Japan, Jun. 2011, pp. 1–5.
[11] V. Pauli, L. Lampe, and R. Schober, "'Turbo DPSK' using soft multiple-symbol differential sphere decoding," *IEEE Trans. Inf. Theory*, vol. 52, no. 4, pp. 1385–1398, Apr. 2006.
[12] C. Leroux, I. Tal, A. Vardy, and W. J. Gross, "Hardware architectures for successive cancellation decoding of polar codes," in *Proc. IEEE Int. Conf. Acoust., Speech Signal Process.*, Prague, Czech Republic, May 2011, pp. 1665–1668.
[13] A. Balatsoukas-Stimming, M. B. Parizi, and A. Burg, "LLR-based successive cancellation list decoding of polar codes," *IEEE Trans. Signal Process.*, vol. 63, no. 19, pp. 5165–5179, Oct. 2015.
[14] E. Arıkan, "Polar Codes: A pipelined implementation," in *Proc. 4th Int. Symp. Broadband Commun.*, Melaka, Malaysia, Jul. 2010, pp. 11–14.
[15] S. Cammerer, M. Ebada, A. Elkelesh, and S. T. Brink, "Sparse graphs for belief propagation decoding of polar codes," in *Proc. IEEE Int. Symp. Inf. Theory*, Vail, CO, USA, Jun. 2018, pp. 1465–1469.
[16] R. H. Clarke, "A statistical theory of mobile-radio reception," *Bell Syst. Tech. J.*, vol. 47, no. 6, pp. 957–1000, Jul./Aug. 1968.
[17] J. Guo, M. Qin, A. G. I. Fàbregas, and P. H. Siegel, "Enhanced belief propagation decoding of polar codes through concatenation," in *Proc. IEEE Int. Symp. Inf. Theory*, Honolulu, HI, USA, Jun./Jul. 2014, pp. 2987–2991.
[18] M. Qin, J. Guo, A. Bhatia, A. G. I. Fàbregas, and P. H. Siegel, "Polar code constructions based on LLR evolution," *IEEE Commun. Lett.*, vol. 21, no. 6, pp. 1221–1224, Jun. 2017.
[19] L. Hanzo, O. Alamri, M. El-Hajjar, and N. Wu, "Turbo detection of channel-coded DSTBC-SP schemes," in *Near-Capacity Multi-Functional MIMO Systems: Sphere-Packing, Iterative Detection and Cooperation*, Chichester, U.K.: Wiley, 2009, pp. 95–124.
[20] L. Li, L. Wang, and L. Hanzo, "Successive AF/DF relaying in the cooperative DS-CDMA uplink: Capacity analysis and its system architecture," *IEEE Trans. Veh. Technol.*, vol. 62, no. 2, pp. 655–666, Feb. 2013.
[21] L. Li, H. V. Poor, and L. Hanzo, "Non-coherent successive relaying and cooperation: Principles, designs, and applications," *IEEE Commun. Surveys Tuts.*, vol. 17, no. 3, pp. 1708–1737, 3rd Quart., 2015.
[22] S. T. Brink, "Convergence of iterative decoding," *Electron. Lett.*, vol. 35, no. 10, pp. 806–808, May 1999.
[23] A. Ashikhmin, G. Kramer, and S. T. Brink, "Extrinsic information transfer functions: Model and erasure channel properties," *IEEE Trans. Inf. Theory*, vol. 50, no. 11, pp. 2657–2673, Nov. 2004.
[24] B. Yuan and K. K. Parhi, "Early stopping criteria for energy-efficient low-latency belief-propagation polar code decoders," *IEEE Trans. Signal Process.*, vol. 62, no. 24, pp. 6496–6506, Dec. 2015.
[25] J. Chen, "Reduced complexity decoding algorithms for low-density parity check codes and turbo codes," Ph.D. dissertation, Dept. Elect. Eng., Univ. Hawaii, Honolulu, HI, USA, 2003.

CHAOFAN CHEN received the B.Eng. degree in communication engineering from Northwest University for Nationalities, Lanzhou, China, in 2012. He is currently pursuing the Ph.D. degree in communication and information system with the School of Information and Electronics, Beijing Institute of Technology, Beijing, China.

His research interests include channel coding and its applications, hardware design and implementation of high-speed decoding, non-coherent detection over coded modulation systems, and non-orthogonal multiple access technologies in wireless communications.

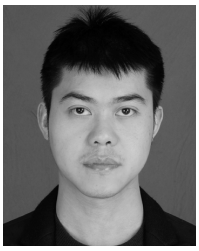

LI LI received the Ph.D. degree from the Southampton Wireless Group, School of Electronics and Computer Science, University of Southampton, in 2013. After completing the Ph.D. degree, he conducted research as a Senior Research Assistant with the School of Electronics and Computer Science, University of Southampton, from 2013 to 2014. In 2015, he joined the Provincial Key Laboratory of Information Coding and Transmission, Southwest Jiaotong University, Chengdu, China, as an Associate Professor.

His research interests include channel coding, iterative detection, noncoherent transmission technologies, cooperative communications, network coding, and non-orthogonal multiple access technologies.

LI WANG (S'09–M'10) was born in Chengdu, China, in 1982. He received the Ph.D. degree from the University of Southampton, Southampton, U.K., in 2010. From 2010 to 2012, he conducted research as a Senior Research Fellow with the School of Electronics and Computer Science, University of Southampton. During his academic period, he was involved in a number of projects, such as those from U.K.'s EPSRC, Mobile VCE, and the India-U.K. Advanced Technology Centre. In 2012, he joined the R&D Center, Huawei Technologies, Stockholm, Sweden, and is currently a Principle Engineer with the Wireless Network Algorithm Laboratory. He has authored over 40 research papers in IEEE/IET journals and conferences and has also co-authored one Wiley/IEEE press book. He research interests include both radio transmission technology and radio resource management areas for future wireless communication technologies and networks, including PHY layer modeling, advanced iterative receiver design, noncoherent transmission techniques, link adaptation, power control, scheduling, cross-layer cross-module system design, CoMP, massive MIMO, mmWave, and communication system intelligentization. He has now been conducting pioneering cross-discipline studies to build next-generation communication systems with artificial intelligence. Upon his significant contributions in this field, he was a recipient of the Huawei Individual Contribution Award, in 2015, and the Furture Star Award, in 2017.

SHUAI WANG received the B.Eng. degree (Hons.) in communications engineering from Zhengzhou University, in 2005, and the Ph.D. degree (Hons.) in communications engineering from the Beijing Institute of Technology, China, in 2012.

From 2010 to 2011, he was a Visiting Ph.D. Student with the School of Electronics and Computer Science, University of Southampton, U.K. He has been with the School of Information Science and Electronics, Beijing Institute of Technology, since 2012, where he is currently an Associate Professor. His research interests include channel estimation, anti-jamming transmission, synchronization techniques, and beamforming. He received the award for outstanding Ph.D. dissertation granted by the Beijing Municipal Education Commission, in 2013, with other 49 co-winners, nominated from all the Ph.D. graduates who received their degree in Beijing that year.

He has published more than 20 peer-reviewed articles, mainly in leading IEEE journals or conferences. He holds 17 patents. He served or serves as the principal investigator for 12 research funds, including two granted by the National Science Foundation of China. He was a recipient of the (Second Class) Scientific and Technical Progress Award granted by the Ministry of Industry and Information Technology of China.

XIANGMING LI received the Ph.D. degree in communication and information engineering from the Beijing University of Posts and Telecommunications, Beijing, China, in 2000. From 2000 to 2002, he was with Agilent Technologies as a Software Engineer. From 2002 to 2003, he was a Postdoctoral Fellow with the Department of Electrical and Computer Engineering, Concordia University, Canada, and with the Department of Electronic Engineering, City University of Hong Kong. From 2003 to 2005, he was an Associate Professor with the School of Communication and Information Engineering, Chongqing University of Posts and Telecommunications, China. From 2006 to 2008, he was with NTT DOCOMO Beijing Communications Laboratories Co. Ltd., as a Researcher and Research Manager. In 2008, he joined the School of Information and Electronics Engineering, Beijing Institute of Technology, where he is currently a Full Professor. His current research interests include wireless and mobile communications, information theory and coding, and information learning.

GEORGE K. KARAGIANNIDIS (M'96–SM'03–F'14) was born in Pythagorion, Greece. He received the University Diploma and Ph.D. degrees in electrical and computer engineering from the University of Patras, in 1987 and 1999, respectively. From 2000 to 2004, he was a Senior Researcher with the Institute for Space Applications and Remote Sensing, National Observatory of Athens, Greece. In 2004, he joined the Faculty of Aristotle University of Thessaloniki, Greece, where he is currently a Professor with the Electrical and Computer Engineering Department and the Director of the Digital Telecommunications Systems and Networks Laboratory. He is also an Honorary Professor with South West Jiaotong University, Chengdu, China.

His research interests include digital communication systems and signal processing with an emphasis on wireless communications, optimal wireless communications, wireless power transfer and applications, molecular and nanoscale communications, stochastic processes in biology, and wireless security.

He has authored or co-authored over 450 technical papers published in scientific journals and presented at international conferences. He has authored the Greek Edition of the book *Telecommunications Systems* and has co-authored the book *Advanced Optimal Wireless Communications Systems* (Cambridge, 2012).

Dr. Karagiannidis has been the general chair, the technical program chair, and a member of technical program committees in several IEEE and non-IEEE conferences. He was an Editor of the IEEE TRANSACTIONS ON COMMUNICATIONS, a Senior Editor of the IEEE COMMUNICATIONS LETTERS, an Editor of the *EURASIP Journal of wireless Communications and Networks*, and a several times Guest Editor of the IEEE SELECTED AREAS IN COMMUNICATIONS. From 2012 to 2015, he was the Editor-in-Chief of the IEEE COMMUNICATIONS LETTERS.

Dr. Karagiannidis is one of the highly cited authors across all areas of electrical engineering and was recognized as a 2015, 2016, and 2017 Web-of-Science Highly Cited Researcher.